Single-Molecule Fluorescence Imaging of DNA at a Potential-Controlled Interface

Eric M. Peterson and Joel M. Harris*
Department of Chemistry, University of Utah, 315 South 1400 East
Salt Lake City, Utah 84112-0850 USA

ABSTRACT

Many interfacial chemical phenomena are governed in part by electrostatic interactions between polyelectrolytes and charged surfaces; these phenomena can influence the performance of biosensors, adsorption of natural polyelectrolytes (humic substances) on soils, and production of polyelectrolyte multi-layer films. In order to understand electrostatic interactions that govern these phenomena, we have investigated the behavior of a model polyelectrolyte, 15 kbp fluorescently labeled plasmid DNA, near a polarized indium tin oxide (ITO) electrode surface. The interfacial population of DNA was monitored *in situ* by imaging individual molecules through the transparent electrode using total-internal-reflection fluorescence microscopy. At applied potentials of +0.8 V versus Ag/AgCl, the DNA interfacial population near the ITO surface can be increased by two orders of magnitude relative to bulk solution. The DNA molecules attracted to the interface do not adsorb to ITO, but rather, they remain mobile with a diffusion coefficient comparable to free solution. Ionic strength strongly influences the sensitivity of the interfacial population to applied potential, where the increase in the interfacial population over a +300-mV change in potential varies from 20% in 30-mM ionic strength to over 25-fold in 300-μM electrolyte. The DNA accumulation with applied potential was interpreted using a simple Boltzmann model to predict average ion concentrations in the electrical double layer and the fraction of interfacial detection volume that is influenced by applied potential. A Gouy-Chapman model was also applied to the data to account for the dependence of the ion population on distance from the electrode surface, which indicates that the net charge on DNA responsible for interactions with the polarized surface is low, on the order of one excess electron. The results are consistent with a small fraction of the DNA plasmid being resident in the double-layer and with counter-ions screening much of the DNA excess charge.

*Corresponding author: E-mail: harrisj@chem.utah.edu

INTRODUCTION

Interactions of charged surfaces with polyelectrolytes and charged particles are important in numerous fields, including environmental science (adsorption of humic substances to oxide surfaces),[1-4] device fabrication (assembly of polyelectrolytes to produce thin films),[5,6] and bioanalytical techniques (reactions of charged biomolecules at sensing surfaces).[7-11] Interactions of polyelectrolytes with surfaces may include hydrophobic, steric, as well as electrostatic contributions;[12] however, because polyelectrolytes can have thousands to millions of charged surface groups, electrostatic interactions with surfaces are expected to be significant. A quantitative understanding of these electrostatic interactions will help describe the affinity of polyelectrolytes for charged interfaces[13,14] or nonspecific interactions in bioanalytical techniques.[15,16]

Significant insight into the potential-dependent behavior of polyelectrolytes in the electrical double-layer near a charged surface could be gained if they are imaged as individual molecules. Total internal reflection fluorescence (TIRF) microscopy[17] allows imaging of fluorescent molecules in a thin (≈150 nm thick) interfacial region near a glass surface illuminated by an evanescent wave from excitation radiation internally reflected at the glass-solution interface. Single molecule fluorescence imaging is a powerful tool for measuring biophysical interactions at solid-liquid interfaces, such as biomolecule-ligand binding,[18,19] biomolecule-surface binding and interactions,[20-22] and protein-protein interactions.[23] Single-molecule imaging has several advantages over bulk techniques for probing chemistry at interfaces. Single-molecule techniques have low detection limits, 10-100 yoctomol,[24,25] which are ideal for observing populations of dilute molecules (pM to nM) in the interfacial region, thus avoiding steric effects either in solution or on the surface. Interfacial populations can be directly determined by counting molecules in images, where no intensity calibration is required.[25]

Interfacial diffusion can be directly determined on an individual molecule basis by tracking the positions of molecules versus time.[26-29] Probing individual molecules also reveals sample heterogeneity that would be lost in bulk techniques which report an ensemble average of molecular behavior.[30,31]

The imaging of individual, fluorescently labeled DNA molecules at liquid-solid interfaces was pioneered by Yeung, Porter, and co-workers who have investigated the interfacial behavior of DNA at self-assembled monolayers on gold,[32,33] at bare glass,[34,35] and at transparent carbon electrodes.[36] At the carbon electrode surface, reversible increases in the interfacial DNA population could be observed under the influence a positive applied potential, showing the utility of this methodology to investigate interfacial electrolyte populations under potential control. Fluorescence experiments performed near thick (opaque) gold metal electrodes have successfully probed the influence of the electrical double-layer on the orientation and conformation of surface-tethered DNA.[37,38]

In the present work, we build on these measurement concepts with a goal of quantifying DNA populations in the double-layer region in response to applied potential. An indium-tin-oxide (ITO) thin film sputter-coated onto glass provides a uniform and highly transparent electrode surface for control of the potential, while simultaneously allowing low-background imaging of individual labeled DNA molecules near the interface. ITO has previously been used in bulk fluorescence measurements to investigate the effect of applied potential on streptavidin-biotin interactions[10] and the accumulation of individual labeled antibodies at a charged surface.[24] Using through-the-objective TIRF microscopy, we quantify the interfacial population of fluorescently labeled DNA at an ITO surface, in response to applied potential at varying electrolyte ionic strengths, by counting individual molecules in fluorescence images. This approach has several advantages relative to interfacial fluorescence intensity measurements.

First, the interfacial population of DNA molecules within the imaging area and evanescent wave depth can be determined directly without calibration so that the potential-dependent accumulation relative to the free-solution concentration can be modeled on an absolute not a relative basis. Secondly, single-molecule counting provides proof that an increase in fluorescence is a result of increasing the DNA population and not potential-dependent changes in the intercalating dye content or quantum efficiency. Finally, single-molecule imaging allows the measurement of diffusion coefficients by tracking of individual molecules in order to investigate whether the DNA is adsorbed to the ITO surface. These results show that, while the interfacial DNA population grows with increasing positive applied potential, DNA molecules attracted to the interface remain mobile, with diffusion coefficients very similar to those measured in free solution. The DNA accumulation with applied potential is first interpreted using a simple Boltzmann model to predict average ion concentrations in the electrical double layer and how the fraction of interfacial detection volume controlled by applied potential varies with ionic strength. A Gouy-Chapman model is also applied to the data to account for the distance dependence of the ion population from the electrode surface. Application of this model to the observed DNA interfacial populations indicates that the DNA within the double-layer exhibits a modest net charge on the order of a single excess electron. The results are consistent with only a fraction of the DNA phosphate groups being resident in the double layer, where screening by counter-ions further reduces the net charge on the molecule.

EXPERIMENTAL SECTION

Chemicals and Material. The 14,876 base pair (bp) supercoiled plasmid, PTX21, (see Supporting Information) was generously provided by the Eric Jorgensen Lab (University of Utah). Oxazole yellow dimer (YOYO-1) iodide DNA intercalating dye (1 mM solution in DMSO) was purchased from Invitrogen (Carlsbad, CA) and used as received. All buffers and solutions were made using water distilled from a quartz still and purified with a Barnstead NANOpure II system (Boston, MA) to a solution resistivity of approximately 18 MΩ·cm. Indium tin oxide (ITO) sputter-coated 20 x 20 mm No. 1 glass coverslips (sheet resistivity of 15-30 Ω/square) were purchased from SPi Supplies (West Chester, PA). Buffers and supporting electrolyte solutions were made with ACS grade sodium phosphate monobasic monohydrate, sodium chloride, and sodium hydroxide from Mallinckrodt (Phillipsburg, NJ). Spectroscopy grade Omnisolv methanol from EMD chemicals (Darmstadt, Germany) was used for cleaning ITO coverslips. Conductive silver epoxy resin was purchased from VWR (West Chester, PA).

DNA Solutions. All solutions used for fluorescence imaging were prepared in sodium phosphate buffer adjusted to pH 8.0 with sodium hydroxide in addition to varying amounts of sodium chloride to control ionic strength. Stock solutions of the 14,876-bp plasmid DNA were prepared with 180 pM DNA, 160 nM YOYO-1 (DNA base pair-to-dye ratio of 15 to 1), 75 μM sodium chloride, and 75 μM sodium phosphate buffer. The DNA-YOYO-1 stock solution was allowed to incubate at room temperature for approximately 4 h to allow the YOYO-1 fluorescent label to intercalate into the double-stranded DNA before being further diluted to concentrations of 5.3, 10.5, 21, and 42 pM in buffers of varying ionic strength. The 10.5, 21, and 42 pM DNA solutions were all prepared in 75 μM phosphate buffer plus sodium chloride electrolyte at 75 μM, 3 mM, or 30 mM, respectively. The 5.3 pM DNA solution was prepared with low concentration electrolyte containing 2.3 μM phosphate buffer and 2.3 μM sodium chloride. The

DNA concentration in solution was varied with ionic strength in order to manage the dynamic range of the molecular counting experiment. At low ionic strengths, the large interfacial concentration increase with applied potential requires that one start at low concentrations to avoid exceeding the maximum number of molecules that can be counted in an image. At higher ionic strengths, the increase in DNA population with applied potential is modest, and a higher starting concentration allows one to measure accurately the smaller relative change.

Preparation of ITO Substrates. ITO electrodes were prepared by first rinsing for 10 min each in 18 MΩ·cm water and methanol. The ITO coated side of the coverslip was then cleaned for 25 min in a UV ozone cleaner, Jelight Co. model 342. Copper wire leads were attached to the edge of the ITO coated coverslip using conductive silver epoxy resin which was then placed in a 120 ºC oven overnight to allow the conductive paste to harden. The slides with attached wire leads were then UV ozone cleaned again for 25 min and assembled into an electrochemical flow cell for imaging, shown in Figure 1. This cell consists of the wired ITO coverslip as a bottom window, separated from a top glass plate by a silicone gasket. The top has inlet and outlet ports that allow solution flow and access by a platinum counter electrode and a Cypress Systems (ESA, inc.) model EE009 Ag/AgCl reference electrode. The flow cell is held together by threaded stainless-steel top and bottom plates whose interior is covered with Parafilm to prevent electrical shorts to ground. A Pine model AFCBP1 3-electrode potentiostat was used to apply surface potentials.

Fluorescence Microscopy. Dilute YOYO-1 labeled DNA solutions at an ITO interface were imaged with an Olympus iX71 inverted microscope that employs through-the-objective TIRF illumination described previously,[25] with several modifications. Briefly, 488-nm illumination from a Coherent Innova 90C argon ion laser is coupled into a polarization maintaining optical fiber (Thorlabs) and directed to the back of the microscope frame. Light

emitted from the fiber is collected and collimated using a plano-convex lens and then passed through a 488 nm laser band-pass filter (Chroma). The laser beam is then focused with another plano-convex lens onto the back focal plane of a 60x 1.45 N.A. oil immersion objective lens, creating a collimated beam emerging from the objective lens. By translating the optical fiber tip horizontally relative to the objective lens optical axis, the angle of the beam emerging from the objective increased until total internal reflection was achieved at the glass-ITO-aqueous interface. The ~200-nm thick ITO film is not expected to impact the ability to generate an evanescent wave at the ITO-aqueous interface according to calculations of the excitation radiation spatial intensity distribution versus incident angle for three-phase dielectric thin film structures.[39] A total laser power of 1 mW was incident on the back of the objective lens, corresponding to approximately 13 Wcm^{-2} at the sample surface. Before any potential-control and imaging experiments were conducted, the ITO surface was poised at 0.8 V versus Ag/AgCl and illuminated with 1 mW 488 nm laser radiation for 30 min to bleach any adsorbed fluorescent impurities. Imaging was performed using an electron multiplying charge coupled device (EMCCD) camera (Andor $iXon^{EM}$+ 897) using a 256 × 256 pixel region of the sensor (area a = 70 × 70 μm region at 60x magnification). Videos were collected by imaging continuously for 140 s with 27.5 ms integration times (36.4 fps) in frame transfer mode with the electron multiplying gain set at 50x. Before imaging experiments were conducted, ITO substrates were covered with blank phosphate buffer, poised at 0.8 V and illuminated with laser radiation for 30 min to photobleach any fluorescent contamination on the surface.

Image Analysis. Image analysis was performed using custom programs written in the Matlab (Mathworks) software environment. Fluorescently-labeled DNA molecules in each image were identified and counted using an algorithm described previously.[25] Molecules in images were identified by locating regions having at least three adjacent pixels with intensity

higher than a detection intensity threshold, $I_{thold} = n_{std}\,\sigma_{bg} + \mu_{bg}$, set at a number, n_{std}, of background standard deviations, σ_{bg}, higher than the mean background intensity, μ_{bg}. Before analysis, the analog-to-digital unit (ADU) intensity was converted to photoelectron counts. The conversion was made using a linear calibration fit to a plot of pixel intensity variance versus mean pixel intensity in ADU generated from flat, white-light images (see Supporting Information).[40]

The detection intensity threshold establishes a depth into solution in the evanescent-wave illumination region that molecules can be detected. The intensity from individual labeled plasmids varies from being indistinguishable from background, when they are far from the glass/solution interface, to some maximum fluorescence intensity from DNA molecules at their distance of closest approach to the surface. The intensity-distance relationship diverges from a simple exponential decay function due to a small fraction of scattered light from the interface penetrating into solution, and the large size of the plasmids relative to the evanescent wave (~400-nm diameter DNA versus $d \approx 150$-nm evanescent sampling depth,[39] see Supporting Information). Detection intensity thresholds were chosen to optimize bright molecules excited in the evanescent wave and minimize counts of molecules illuminated by scattered light far from the interface. The process used to optimize the detection threshold intensity I_{thold} and its effects on the fitted parameters of the detected population are presented in Supporting Information. The optimum detection threshold for videos acquired at different DNA concentrations varied slightly, from $n_{std} = 5.1$ to 6.7, depending on their signal-to-noise ratios. At detection thresholds, $n_{std} > 5$, the false positive rate is expected to be negligible.[25] Due to this high detection threshold and photobleaching prior observation, less than 0.03 spots per video frame were detected in blanks.

Populations of counted DNA molecules in images, measured as a function of ionic strength and applied potential, were fit to Boltzmann and Guoy-Chapman models (see below), by

optimizing the parameters in the model by non-linear least squares. Uncertainties in reported parameters were estimated using the bootstrap method,[41] generated by adding randomized residuals to a best fit curve. The residuals are inversely weighted by Poisson-distributed molecular shot noise, where the standard deviation, σ_N, of the number of detected molecules is given by the square root of the molecular count, $(N_{DET})^{1/2}$.[42] Standard deviations of each parameter were estimated by fitting a Gaussian distribution to a histogram of bootstrap-determined parameter values. The uncertainties in the reported parameters and error bars in the plots represent two standard deviations of the mean.

Diffusion coefficients for DNA at the interface were determined by tracking the intensity center-of-mass of individual molecules with sub-pixel precision. Because the size of the DNA molecule in solution is larger than the point spread function of the microscope (previously determined[25]) and because the DNA diffuses during an image acquisition, a method of determining the location of the molecule must account for the spatial distribution of DNA in the image and its motion during acquisition. The center-of-mass of the intensity distribution provides a good estimate of the molecule location because the measured intensity is proportional to the spatial distribution of molecular density averaged over the acquisition time. Single molecule trajectories were generated by identifying a molecule coordinate at the beginning of the video and searching for another molecule coordinate in the subsequent frame within a critical radius of 1.3 μm of the initial coordinate. This process was repeated using the new coordinate in the next video frame until no additional coordinates were located, indicating that the molecule had diffused out of the evanescent wave. The critical radius of 1.3 μm is set to be equal to four times the root-mean-squared step size for DNA diffusing in free solution (see below). Even if DNA diffusion at the interface is as fast as in free solution, this critical radius would capture 99.95% of the steps in a trajectory based on a random walk model[30] and provide an unbiased

estimate of the diffusion coefficient. To reduce the probability of collecting spurious steps due to jumps between different molecules in an image that happen to be within the critical radius, only video frames with fewer than 40 counted molecules were used for tracking, typically the first 3 to 15 s of each accumulation. For an image area, a = 4,900 μm^2 (70 × 70 μm), and a critical area of 5.3 μm^2 (1.3 μm critical radius), the probability of a molecule randomly appearing in the critical radius of another molecule from the previous frame is small, less than 4.3%, which is determined from the ratio of the critical area to the total image area, multiplied by the total number of molecules in the image.

RESULTS AND DISCUSSION

Counting DNA Populations near an ITO Interface. The effect of applied potential on the interfacial population of YOYO-1 labeled 14,876-bp supercoiled plasmid DNA is illustrated by data in Figure 2a, which shows raw fluorescence images of DNA in pH 8.0 buffer in the evanescent excitation region near an ITO electrode surface, acquired ~120 s after applying potentials that vary between 0 and +0.9 V versus a Ag/AgCl reference electrode. Under positive applied potential, the population of DNA at the interface increases dramatically, up to a factor of 200 times the interfacial population observed at open circuit. The potential response is fully reversible, and all DNA molecules remain mobile, as long as the applied potential remains below ~1.4 V. For example, when the potential is stepped from 0 V to 1.3 V and then back to 0 V, the population of molecules rises and then declines to its original value within ~5 seconds after the potential is switched back to 0 V (see movie in Supporting Information). The mobility of the interfacial DNA (which is only slightly smaller than its diffusion in free solution, see below) and the immediate reversibility of the interfacial population are consistent with accumulation of DNA in the diffuse double layer and not adsorption to the ITO surface. This behavior stands in

Stark contrast with the potential being stepped to higher than 1.4 V, where a significant population of DNA adsorbs irreversibly. Under these conditions (see Supporting Information), the DNA loses mobility and does not leave the interface upon reversal of the potential, both signatures of strong adsorption to the ITO surface.

From fluorescence images like those in Figure 2(a), interfacial populations of YOYO-1 labeled DNA were determined using an image analysis routine that requires molecular spots to exceed an intensity threshold in multiple adjacent pixels, to distinguish DNA spots from single-pixel detector noise (see above). Figure 2(b) shows DNA molecules detected in a representative image of 10.5 pM DNA solution in 0.28 mM ionic strength electrolyte at an applied potential of 0.8 V. The influence of any free YOYO-1 on these results was tested in a control experiment, where the dye was present at the same total concentration and no DNA was in solution. The number of counted spots averaged 0.03 per frame, which is an equivalent background count rate as observed for ITO slides in a blank buffer solution (see above). The small background count is negligible compared to the 20 to 300 molecules per frame (depending on potential) counted when DNA is present. Thus, the molecular counts are dominated by DNA, which were determined 120 s after each potential step, averaging the molecule counts in the subsequent 500 frames, or 13.8 s. The average numbers of detected DNA molecules in the interface, N_{DET}, are plotted versus applied potential in Figure 3(a-d), for ionic strengths of 8.4 μM, 0.28 mM, 3.2 mM and 30 mM and bulk DNA concentrations of 5.3, 10.5, 21, and 42 pM, respectively. These plots show the strong dependence of the interfacial population on applied potential, especially at low ionic strengths.

Mobility of Interfacial DNA under Potential Control. In order to interpret the interfacial populations of DNA versus applied potential, it is important to ascertain whether these molecules reside in solution, where a double-layer model might be employed for the population

analysis, or whether the molecules spend a significant fraction of time adsorbed to the electrode surface. If the accumulation of DNA involves adsorption to the ITO surface, then the diffusion coefficient of DNA should decrease significantly with increasing positive potential. By tracking the locations of individual molecules through a sequence of video frames, one can measure the diffusion coefficient of DNA at the ITO-solution interface and its dependence on applied potential. The same video data used for counting DNA populations were further analyzed to determine the trajectories of individual molecules. The center-of-mass of the intensity distribution of each molecular spot was tracked with sub-pixel (< 260-nm) resolution. From the resulting trajectories, the mean square displacement, $\langle \Delta r^2 \rangle = \langle \Delta x^2 + \Delta y^2 \rangle$, was determined and plotted versus elapsed time, t. The resulting plots are linear (see Supporting Information) as expected from the Einstein equation in two dimensions: $\langle \Delta r^2 \rangle = 4Dt$. From the slopes of these plots, the interfacial diffusion coefficient of labeled DNA versus applied potential was determined at ionic strengths of 8.4 μM, 0.28 mM, and 3.2 mM and the results are plotted in Figure 4, and summarized in Table 1.

For comparison, the diffusion coefficient of YOYO-1 labeled DNA diffusing in free solution was also measured using an epi-illumination fluorescence microscope focused approximately 10 μm beyond a glass coverslip in solution. The details of the instrumentation and experiment are summarized in Supporting Information, along with plots of mean squared molecule displacement, $\langle \Delta r^2 \rangle$, versus elapsed time, t, for the same supercoiled plasmid DNA at 0.28 mM ionic strength. From these results, the diffusion coefficient of the labeled DNA in free solution was determined to be $D = 1.11\ (\pm\ 0.03) \times 10^{-8}\ \mathrm{cm^2 s^{-1}}$. This diffusion coefficient is somewhat lower than other estimates for DNA of similar molecule weight,[29,43-45] possibly due to the lower ionic strength conditions and the intercalating fluorescent label reducing the supercoiling and compactness of the DNA.[46] The hydrodynamic size of the DNA can be

expressed as an equivalent hard-sphere diameter in solution and estimated from the Stokes-Einstein relationship, where the equivalent diameter is given by $(kT/3\pi\eta D)$ = 400 (± 10) nm, assuming a solution viscosity of pure water, η = 0.89 cP. The validity of the tracking experiment in reporting hard-sphere sizes was verified by measuring the diffusion coefficients of several fluorescently labeled latex spheres of known diameter, and the results are found in Supporting Information.

Diffusion coefficients of labeled DNA in the evanescent wave region near the electrode surface are plotted in Figure 4 as a function of applied potential, and the results are summarized for each ionic strength in Table 1. A slight increase in *D* is observed with increasing electrolyte ionic strength, which is likely due to compaction of the DNA random coil as electrostatic repulsion between phosphate groups is screened by excess electrolyte.[47] Comparing behavior at the same ionic strength (0.28 mM), the diffusion coefficient of DNA in the interfacial region is *D* = 0.88 (± 0.03) × 10^{-8} cm^2s^{-1}; this result is only 20% smaller than the diffusion coefficient measured in free solution under the same conditions, 1.11 (± 0.03) × 10^{-8} cm^2s^{-1}. We conclude, therefore, that DNA in the evanescent wave remains nearly as mobile as in free solution, with only occasional contact with the electrode surface. Furthermore, as shown by the results in Figure 4, there is no trend in the diffusion coefficient with applied potential, matching behavior previously reported for DNA near optically transparent carbon electrodes.[36] This result indicates that DNA plasmids are not deformed sufficiently by moderate fields to denature and adsorb to the ITO surface, even with applied potentials as high as 0.9 V where the diffusion coefficient can be measured. At potentials above 0.9 V, the interfacial DNA population densities become too high for tracking of individual molecules; however, the molecular spots remain mobile even at potentials has high as 1.3 V, as shown in video in Supporting Information.

Boltzmann Model for the Response of Interfacial DNA Populations to Applied Potential. Because applied potentials between 0.7 and 1.3 V greatly increase the interfacial population of DNA, while having no significant influence on diffusion near the interface, the data suggest that the DNA remains in solution and accumulates in the electrical double layer formed at the polarized ITO-aqueous interface. The negatively charged DNA gathers at the interface because of electrostatic attraction to the positive electrode potential, while lateral diffusion, parallel to the electrode surface, is unaffected by applied potential because there is no potential gradient in the interfacial plane. A simple Boltzmann model was developed to account for the potential-dependent accumulation of DNA in the electrical double layer at the ITO interface.

The model begins with Gouy-Chapman theory, which describes the electrical potential and ion concentration in the diffuse double layer. The Gouy-Chapman potential profile, $\varphi(x)$, in the low potential limit decays exponentially into solution from the electrode surface, x:[48,49]

$$\varphi(x) = \varphi^0 \mathrm{e}^{-\kappa x} \tag{1}$$

The dimensions of the electrical double layer are conveniently described by the Debye length, κ^{-1}, the decay constant of the potential profile. The Debye length for a 1:1 electrolyte is a function of the bulk ion concentration, C^0, the ion charge, z, the elementary charge, e, the electrical permittivity of a vacuum, ε_0, the relative permittivity, ε, Boltzmann's constant, k, and the solution temperature, T, given by:

$$\kappa^{-1} = \left(\frac{\varepsilon\varepsilon_0 kT}{2C^0 z^2 e^2}\right)^{1/2} \tag{2}$$

The spatial profile of the number density of ions in the double layer, $n(x)$, depends on the local potential, $\varphi(x)$, and the number density of ions in bulk solution far from the surface, n^0:

$$n(x) = n^0 \mathrm{e}^{-\frac{ze\varphi(x)}{kT}} \quad (3)$$

Because the DNA plasmids investigated are polyanions, they are expected to exhibit electrostatic Boltzmann accumulation near a charged interface. The potential profile of the electrical double layer for real systems at large applied potentials arises from complex ion distributions[50] and even changes in solvent structure.[51] We simplify this model by defining an average concentration of DNA within the double layer, $\langle n_D \rangle$, where the effect of the applied electrical potential, φ, on the population is captured in a Boltzmann parameter, β, describing the sensitivity of the population to changes in applied potential:

$$\langle n_D \rangle = n^0 \mathrm{e}^{-\beta\,\varphi} \quad (4)$$

where β captures the fall-off in potential over the region of the double layer sampled by DNA; for a population of ions at the electrode surface ($x = 0$), the upper bound to the parameter is $\beta \leq Ze/kT$, where Z is the net charge (see Equation 3).

To represent the total number of DNA molecules imaged within the double-layer region, we multiply $\langle n_D \rangle$ by the Debye length κ^{-1} and the area of an image frame, a, and obtain expressions for the DNA population imaged within the double-layer under applied potential, $N_D = \kappa^{-1}\, a\, \langle n_D \rangle$, where the DNA population within the double-layer at zero surface potential (zero net charge) is $N_D^0 = \kappa^{-1}\, a\, n^0$:

$$N_D = N_D^0 \mathrm{e}^{-\beta\,\varphi} \quad (5)$$

Because the evanescent wave penetration depth, d = 150 nm, is larger than the Debye lengths (2 to 100 nm) for the ionic strengths used, not all detected molecules are expected to be under potential control. For this reason, N_D only describes the DNA population in the double layer region. The DNA population in the absence of an interfacial potential in the entire

evanescent wave detection volume is $N_E^0 = d\ a\ n^0$, so that the DNA population outside the double layer (unaffected by applied potential) but inside the evanescent wave detection volume is $N_E^0 - N_D^0$. The total DNA population predicted within the evanescent wave detection volume by this Boltzmann model, N_B, is the sum of N_D and $N_E^0 - N_D^0$:

$$N_B = (N_E^0 - N_D^0) + N_D^0 e^{-\beta\varphi} \quad (6)$$

The interfacial DNA population is governed by the electrical potential at the distance of closest approach for ions at the electrode surface. This distance, the outer Helmholtz plane (OHP), represents the thickness of an adsorbed layer of water and ions. The potential term from Equation 6 must be modified to include the potential applied by the potentiostat, *E*, and an offset, the threshold OHP potential, φ_{OHP}^0, representing the potential required to generate zero net charge at the OHP. The threshold OHP potential is similar to the potential of zero charge (φ_{PZC}); φ_{PZC} is the potential required to neutralize all charge on the *electrode* side of the interface, while φ_{OHP}^0 is the potential which neutralizes charge on the *solution* side of the interface. When $E = \varphi_{PZC}$ the potential in the electrical double layer is not zero, due to excess charge from specifically adsorbed ions and charged groups on the ITO surface. Additional applied potential, $E = \varphi_{OHP}^0$, is required to neutralize this excess surface charge so that the net potential accessible to ions in solution is proportional to $(E - \varphi_{OHP}^0)$. The OHP potential, however, is not exactly equal to $(E - \varphi_{OHP}^0)$, because of the potential drop across the Stern layer. This potential drop is captured by the empirical Boltzmann sensitivity parameter, β.

These modifications to the average potential term lead to Equation 7, which describes the detected interfacial DNA population in the evanescent wave region as a function of applied potential:

$$N_{\mathrm{B}} = (N_{\mathrm{E}}^{0} - N_{\mathrm{D}}^{0}) + N_{\mathrm{D}}^{0}\mathrm{e}^{-\beta(E-\varphi_{\mathrm{OHP}}^{0})} \quad (7)$$

Using a non-linear least-squares parameter search, N_{B} from Equation 8 was fit to the *measured* DNA population, N_{DET}, to estimate values for N_{E}^{0}, N_{D}^{0}, β and $\varphi_{\mathrm{OHP}}^{0}$, and the results are plotted in Figure 3(a-d), with fitted parameters listed in Table 1. The relative DNA population excess in the double layer, can be determined from $[N_{\mathrm{DET}} - (N_{\mathrm{E}}^{0} - N_{\mathrm{D}}^{0})]/\ N_{\mathrm{D}}^{0}$. These results are summarized in Figure 3(e) and fit to the Boltzmann factor from Equation 7, exp $[-\beta\ (E - \varphi_{\mathrm{OHP}}^{0})]$. The results demonstrate the sensitivity of DNA accumulation to ionic strength, where at lower ionic strengths, the double-layer extends further into solution, the DNA population experiences greater attraction to the interface at positive applied potentials.

The sensitivity of the DNA population to applied potential is captured by the Boltzmann potential parameter, β in V^{-1}, the values of which are listed in Table 1 and plotted verses the Debye length, κ^{-1} in nm, in Figure 5. As shown by the results, the parameter β varies significantly with electrolyte concentration and Debye length. For large κ^{-1} at lower ionic strengths, the DNA population exhibits a greater increase with applied potential than for short κ^{-1} because the double layer can influence a larger fraction of the DNA molecular volume and counter-ion screening should be less significant. For all Debye lengths, β is less than 38.9 V^{-1} in magnitude, the sensitivity expected for a monovalent ion experiencing the full applied potential at the ITO surface. The results are consistent with DNA exhibiting a small net charge and experiencing only a small fraction of the applied potential.

As the Debye length increases, not only should the potential sensitivity increase as discussed above, but the fraction of DNA molecules in the evanescent wave detection region that are also within the double layer should also rise. To test this hypothesis, the ratio $N_{\mathrm{D}}^{0}/N_{\mathrm{E}}^{0}$, the fraction of detected molecules that experience the applied potential, was plotted versus the

Debye length, and the results are shown in Figure 6. The increasing trend in N_D^0/N_E^0 with κ^{-1} is a result of the double-layer region encompassing a larger fraction of the evanescent-wave detection volume. Extrapolation of the roughly linear trend in N_D^0/N_E^0 to unity, suggests an evanescent wave sampling depth of ~220 nm, somewhat larger than the evanescent-wave depth of ~150 nm predicted from the refractive indices of glass and solution and the angle of incidence.[39] The evanescent-wave sampling depth can also be estimated by determining the distance into solution required to supply N_E^0 molecules to a 70-μm × 70-μm image area at a given DNA concentration. The average sampling depth estimated from the fitted values of N_E^0 at four DNA concentrations is d = 410 ± 260 nm (95% confidence). While this result is significantly larger than the evanescent-wave depth of ~150 nm expected from the angle of incidence,[39] the result includes the expected value within its large uncertainty bounds. Anomalously high numbers of YOYO-1 labeled DNA diffusing near silica surfaces have also been reported by He *et al.*,[35] and those results corresponded to sampling depths between 500 to 800 nm, or 3 to 6 times greater than the evanescent wave depth of 140 nm. These elevated molecule counts were attributed to diffusion of DNA into and out of the evanescent-wave region during the 257-ms image integration times and confirmed with random-walk simulations. This phenomenon should have less impact on the present experiments because the integration times were only 26 ms, which reduces the distance over which DNA can diffuse during the acquisition of an image by a factor of $(1/10)^{1/2}$ or 0.32. Excess molecular population at the interface may also arise simply from the large size of the DNA molecules. The hard-sphere equivalent diameter of the DNA determined from its solution diffusion coefficient is 400 nm (see Supporting Information), and it is highly labeled. Therefore, it is possible for DNA with a center of mass hundreds of nanometers away from the surface to have labeled base pairs inside the evanescent-wave region. Because of the size of DNA and its possible diffusion within the observation time, the population of DNA, N_E^0, sampled within the

evanescent-wave region will likely include molecules whose center-of-mass distances from the ITO surface exceed 150 nm. In future work, it would useful to employ prism-based TIRF for excitation[35] so that the angle of incidence and evanescent-wave depth could be varied to further characterize the distance dependence of the interfacial DNA population.

The final parameter of the DNA accumulation fit to equation 4 is the threshold OHP potential, φ^0_{OHP}, which increases from 0.59 V to 0.80 V for 8.4 μM to 30 mM ionic strengths respectively, as listed in Table 1. The relatively high positive φ^0_{OHP} for these ITO surfaces in contact with pH 8.0 buffer indicates that there is net negative charge on the surface that must be overwhelmed with a positive applied potential before DNA begins to accumulate. This result is consistent with negative zeta potentials observed for aqueous ITO colloids at pH higher than their isoelectric pH of 5 to 6.[52,53] The increasing trend in φ^0_{OHP} may be a result of increasing chloride ion adsorption to the electrode surface at high electrolyte concentrations requiring higher applied potential to overcome the additional negative surface charge.

Effective DNA Charge Responsible for Ion Accumulation in the Electrical Double-Layer. The simple Boltzmann model of Equation 7 describes both the DNA potential sensitivity and fraction of DNA under potential control as averages over the Debye length. While spatial averaging captures the average population behavior with applied potential, it neglects the distance dependence of ion build-up in the diffuse double-layer. To estimate the effective DNA charge responsible for the observed population, a model is needed that accounts for the potential distribution in the double layer and integrates ion concentrations as they vary with distance from the ITO surface. From a double-layer model, one can directly compare DNA accumulation to the predicted electrolyte ion accumulation and thus estimate the net electrical charge on DNA.

We employ a simple Gouy-Chapman model to describe ionic strength dependence of DNA accumulation in the double-layer: DNA concentration is modeled by numerically

integrating the Boltzmann distribution for the ion concentration profile from the ITO surface to the evanescent-wave depth of 150 nm. The ion profile, adapted from Equation 3, is integrated and multiplied by the image area to provide an expression for the total number of molecules predicted by the Gouy-Chapman model, N_{GC}:

$$N_{GC} = a\int_0^d n^0 \mathrm{e}^{\frac{-Ze\varphi(x)}{kT}} dx \tag{9}$$

The potential distribution, $\varphi(x)$, is approximated with an exponential decay function, Equation 1, using decay constants, κ, calculated from Equation 2 for each ionic strength. Potential at the interface, φ^0, is defined as $E - \varphi^0_{OHP}$, where values for φ^0_{OHP}were taken from fits of the data to Equation 7:

$$\varphi(x) = (E - \varphi^0_{OHP})e^{-\kappa x} \tag{10}$$

DNA net charge, Z, is the only parameter optimized in a fit of N_{GC} to the experimental DNA accumulation curves, N_{DET}, normalized to N_E^0, where values for N_E^0 were also taken from fits of the data to Equation 7. As shown in Figure 7, the model fits the data quite well with, DNA net charges that vary between Z = −0.8 and −0.6 for low to high ionic strengths. Fortunately, these results are not very sensitive to the sampling depth, d, which governs both N_E^0 and the integration of charge in the double layer. If d is increased from the expected evanescent wave depth of 150 nm to the experimental result of 410 nm (determined from N_E^0 results, see above), the DNA net charge increases by only 20%, ranging from Z = −0.96 to −0.79 for low to high ionic strengths, respectively.

Estimates of the effective charge of DNA vary in the literature, ranging from 0.06 electron equivalents *per base* measured for DNA in an agarose gel stretched under electrophoresis conditions,[54] to 0.08 − 0.6 electron equivalents per base measured in capillary

zone electrophoresis.[55,56] Both of these observations predict significant charge on large oligonucleotides. The static double-layer accumulation measurements in the present work have several key differences compared with electrophoresis experiments. First, while the DNA contains thousands of charged phosphate groups, the molecule is large relative to the Debye length, so that only a small fraction of a DNA molecular volume (for example, 0.05% or 7 phosphate groups based on a uniform spherical model of DNA at 3.2-mM ionic strength) resides in the double-layer. The phosphate charges that manage to penetrate the double-layer, however, must still be largely screened by counter-ions to exhibit such a small (fractional) net charge. The screening in this static accumulation experiment differs from electrophoresis, where in the latter case counter-ions in the diffuse layer around polyelectrolytes are sheared away as they migrate in the opposite direction due to their opposite charge. The zeta potential, which determines the magnitude of the electrophoretic mobility, is the potential at the "slip plane" where counter-ions are sheared away. The slip, or shear, plane is thought to be slightly beyond a stagnant water layer several angstroms thick adsorbed to the outer Helmholtz plane. At ionic strengths below 100 mM, this shear plane is within the diffuse double-layer, and the surface charge on the polyelectrolyte is screened primarily by adsorbed ions in the Stern layer. In the present, static double-layer accumulation experiment, there is no electrophoresis and no shearing of counter-ions. The counter-ions in the diffuse layer are still present as a DNA molecule approaches the surface, and they significantly screen the DNA surface charge. Additional screening is contributed by the cationic YOYO-1 dye label; however, based on the 1:15 dye-to-DNA base-pair stoichiometry (see above), the dye label is neutralizing no more than 13% of the charge on the sugar-phosphate backbone.

A detailed description of interacting double-layers in the absence of shear or flow is provided by Derjaguin and Landau, Verwey and Overbeek (DLVO) theory,[57,58] which has been

applied to the case of hard spheres approaching a charged interface.[59] Bhattacharjee et al. calculate the potential profile for small particles of radius comparable to κ^{-1} and surface electrical potential of 25 mV approaching a charged interface of the same potential. Maximum interaction potentials for particles close to the charged interface are only a few *kT*, indicating that most of the total charge is screened by counter-ions. An exact DLVO description of polyelectrolytes such as DNA is difficult because these molecules have no definite surface boundary or charge density, but the results of this theory for simple spherical colloids are entirely consistent with the DNA accumulation results.

Summary. Using single-molecule fluorescence microscopy techniques, we have measured the effects of applied potential and electrolyte ionic strength on the interfacial population and diffusional behavior of DNA. Fluorescently labeled DNA plasmids were imaged near a transparent indium tin oxide electrode surface while interfacial electrical potential was varied between 0 and 1.0 V. For potential steps greater than ~0.5 V versus Ag/AgCl, DNA populations increase exponentially with applied potential, and this accumulation process is reversible. Diffusion at the interface was investigated by tracking single-molecule trajectories at the interface, and no potential dependence was observed. Interfacial diffusion coefficients were comparable to bulk diffusion coefficients, indicating that the DNA does not significantly adsorb to the surface as it accumulates at the interface. At high applied potentials, we hypothesize that the DNA gathers at the interface due to attractive electrostatic interactions with the electrical double layer. Plots of interfacial DNA population versus potential were fit by a Boltzmann model with parameters for the fraction of the DNA population under potential influence, the outer Helmholtz plane zero potential, and the potential sensitivity of the DNA potential response. As ionic strength is decreased, the corresponding increase in the double-layer thickness increased both the fraction of observed DNA molecules under potential control, and the sensitivity of the

population to applied potential. A Gouy-Chapman model of ion accumulation in the double-layer accounted for the spatial distribution of potential away from the electrode surface and was integrated to estimate the number DNA molecules within the evanescent detection volume based on their net charge; the results suggest that DNA molecules in the double-layer exhibit a low net charge, between 0.6 and 0.8 electron equivalents. While there is significant charge associated with the phosphate-sugar backbone (~30,000 electron equivalents), only a small fraction of the DNA volume can reside within the double-layer region, and what is present is largely screened by counter-ions. The large DNA plasmid, therefore, interacts only weakly with the applied potential and remains nearly as mobile as in free solution based on its lateral diffusion behavior.

The present results indicate that variation in surface potential can strongly influence interfacial populations of DNA in the double layer without leading to irreversible adsorption to the electrode surface. These results could impact the response of DNA sensors that use applied potentials to electrochemically control binding and denaturation (melting) in DNA sensor applications.[60,61] Application of moderate positive potentials could attract higher concentrations of target single-stranded DNA into the double-layer relative to bulk solution, leading to faster association rates from the higher local concentrations in the interface. Based on the results shown in Figures 5 and 6, attraction of DNA to the interface should only be significant at lower ionic strength conditions and correspondingly longer Debye lengths, where the potential profile can reach further into solution. Most DNA hybridization experiments, however, are carried out at higher ionic strengths (>100 mM) in order to avoid electrostatic repulsion between ssDNA strands that would inhibit hybridization.[62] Under these conditions, the potential-dependent build-up of an interfacial population would be relatively small; see Figure 3(d). In applications to other polyelectrolytes under lower ionic strength conditions (protein biosensors, adsorption of humic substances, layer-by-layer polyelectrolyte deposition), the influence of surface potential

either electrically controlled or influenced by specifically adsorbed ions could play an important role in governing local interfacial concentrations of polyelectrolytes in the double layer.

Supporting Information. This information includes a diagram of the PTX21 plasmid, the intensity conversion to photoelectrons, determination of interfacial and free-solution DNA diffusion coefficients with a comparison to size standards, setting intensity thresholds for single-molecule detection, and DNA accumulation movies. This material is available free of charge via the Internet at http://pubs.acs.org.

Acknowledgment. This research was supported in part with funds from the U.S. Department of Energy under Grant DE-FG03-93ER14333.

REFERENCES

1. Vermeer, A. W. P.; van Riemsdijk, W. H.; Koopal, L. K., Adsorption of Humic Acid to Mineral Particles. 1. Specific and Electrostatic Interactions. *Langmuir* **1998,** 14, (10), 2810-2819.

2. Kaneco, S.; Itoh, K.; Katsumata, H.; Suzuki, T.; Masuyama, K.; Funasaka, K.; Hatano, K.; Ohta, K., Removal of Natural Organic Polyelectrolytes by Adsorption onto Tobermorite. *Environmental Science & Technology* **2003,** 37, (7), 1448-1451.

3. Weng; Van Riemsdijk, W. H.; Koopal, L. K.; Hiemstra, T., Adsorption of Humic Substances on Goethite: Comparison between Humic Acids and Fulvic Acids†. *Environmental Science & Technology* **2006,** 40, (24), 7494-7500.

4. Yang, K.; Lin, D.; Xing, B., Interactions of Humic Acid with Nanosized Inorganic Oxides. *Langmuir* **2009,** 25, (6), 3571-3576.

5. He, J.-A.; Mosurkal, R.; Samuelson, L. A.; Li, L.; Kumar, J., Dye-sensitized Solar Cell Fabricated by Electrostatic Layer-by-Layer Assembly of Amphoteric TiO2 Nanoparticles. *Langmuir* **2003,** 19, (6), 2169-2174.

6. Han, J.; Kim, H.; Kim, D. Y.; Jo, S. M.; Jang, S.-Y., Water-Soluble Polyelectrolyte-Grafted Multiwalled Carbon Nanotube Thin Films for Efficient Counter Electrode of Dye-Sensitized Solar Cells. *ACS Nano* **2010,** 4, (6), 3503-3509.

7. Kalb, E.; Engel, J.; Tamm, L. K., Binding of proteins to specific target sites in membranes measured by total internal reflection fluorescence microscopy. *Biochemistry* **1990,** 29, (6), 1607-1613.

8. Haeussling, L.; Ringsdorf, H.; Schmitt, F. J.; Knoll, W., Biotin-functionalized self-assembled monolayers on gold: surface plasmon optical studies of specific recognition reactions. *Langmuir* **1991,** 7, (9), 1837-1840.

9. Altschuh, D.; Dubs, M. C.; Weiss, E.; Zeder-Lutz, G.; Van Regenmortel, M. H. V., Determination of kinetic constants for the interaction between a monoclonal antibody and peptides using surface plasmon resonance. *Biochemistry* **1992,** 31, (27), 6298-6304.

10. Asanov, A. N.; Wilson, W. W.; Oldham, P. B., Regenerable Biosensor Platform: A Total Internal Reflection Fluorescence Cell with Electrochemical Control. *Analytical Chemistry* **1998,** 70, (6), 1156-1163.

11. Liu, J.; Eddings, M. A.; Miles, A. R.; Bukasov, R.; Gale, B. K.; Shumaker-Parry, J. S., In Situ Microarray Fabrication and Analysis Using a Microfluidic Flow Cell Array Integrated with Surface Plasmon Resonance Microscopy. *Analytical Chemistry* **2009,** 81, (11), 4296-4301.

12. Claesson, P. M.; Go¨lander, C.-G., Direct measurements of steric interactions between mica surfaces covered with electrostatically bound low-molecular-weight polyethylene oxide. *Journal of Colloid and Interface Science* **1987,** 117, (2), 366-374.

13. Murphy, E. M.; Zachara, J. M.; Smith, S. C., Influence of mineral-bound humic substances on the sorption of hydrophobic organic compounds. *Environmental Science & Technology* **1990,** 24, (10), 1507-1516.

14. Jones, K. D.; Tiller, C. L., Effect of Solution Chemistry on the Extent of Binding of Phenanthrene by a Soil Humic Acid: A Comparison of Dissolved and Clay Bound Humic. *Environmental Science & Technology* **1999,** 33, (4), 580-587.

15. Sofia, S. J.; Premnath, V.; Merrill, E. W., Poly(ethylene oxide) Grafted to Silicon Surfaces: Grafting Density and Protein Adsorption. *Macromolecules* **1998,** 31, (15), 5059-5070.

16. Schlapak, R.; Armitage, D.; Saucedo-Zeni, N.; Hohage, M.; Howorka, S., Dense Passivating Poly(ethylene glycol) Films on Indium Tin Oxide Substrates. *Langmuir* **2007,** 23, (20), 10244-10253.

17. Axelrod, D., Total Internal Reflection Fluorescence Microscopy. *Methods in Cell Biology* **1989,** 30, 245-270.

18. Wayment, J. R.; Harris, J. M., Biotin−Avidin Binding Kinetics Measured by Single-Molecule Imaging. *Analytical Chemistry* **2008,** 81, (1), 336-342.

19. Elenko, M. P.; Szostak, J. W.; van Oijen, A. M., Single-Molecule Imaging of an in Vitro-Evolved RNA Aptamer Reveals Homogeneous Ligand Binding Kinetics. *Journal of the American Chemical Society* **2009,** 131, (29), 9866-9867.

20. Liang, H.; Cheng, X.; Ma, Y., Localized Single Molecule Isotherms of DNA Molecules at Confined Liquid−Solid Interfaces. *Analytical Chemistry* **2009,** 81, (6), 2059-2066.

21. Fox, C. B.; Wayment, J. R.; Myers, G. A.; Endicott, S. K.; Harris, J. M., Single-Molecule Fluorescence Imaging of Peptide Binding to Supported Lipid Bilayers. *Analytical Chemistry* **2009,** 81, (13), 5130-5138.

22. Myers, G. A.; Gacek, D. A.; Peterson, E. M.; Fox, C. B.; Harris, J. M., Microscopic Rates of Peptide–Phospholipid Bilayer Interactions from Single-Molecule Residence Times. *Journal of the American Chemical Society* **2012,** 134, (48), 19652-19660.

23. Miyake, T.; Tanii, T.; Sonobe, H.; Akahori, R.; Shimamoto, N.; Ueno, T.; Funatsu, T.; Ohdomari, I., Real-Time Imaging of Single-Molecule Fluorescence with a Zero-Mode Waveguide for the Analysis of Protein−Protein Interaction. *Analytical Chemistry* **2008,** 80, (15), 6018-6022.

24. Li, L.; Tian, X.; Zou, G.; Shi, Z.; Zhang, X.; Jin, W., Quantitative Counting of Single Fluorescent Molecules by Combined Electrochemical Adsorption Accumulation and Total Internal Reflection Fluorescence Microscopy. *Analytical Chemistry* **2008,** 80, (11), 3999-4006.

25. Peterson, E. M.; Harris, J. M., Quantitative Detection of Single Molecules in Fluorescence Microscopy Images. *Analytical Chemistry* **2010,** 82, (1), 189-196.

26. Smith, D. E.; Perkins, T. T.; Chu, S., Dynamical Scaling of DNA Diffusion Coefficients. *Macromolecules* **1996,** 29, (4), 1372-1373.

27. Ke, P. C.; Naumann, C. A., Single Molecule Fluorescence Imaging of Phospholipid Monolayers at the Air−Water Interface. *Langmuir* **2001,** 17, (12), 3727-3733.

28. Ludes, M. D.; Wirth, M. J., Single-Molecule Resolution and Fluorescence Imaging of Mixed-Mode Sorption of a Dye at the Interface of C18 and Acetonitrile/Water. *Analytical Chemistry* **2002,** 74, (2), 386-393.

29. McHale, K.; Mabuchi, H., Precise Characterization of the Conformation Fluctuations of Freely Diffusing DNA: Beyond Rouse and Zimm. *Journal of the American Chemical Society* **2009,** 131, (49), 17901-17907.

30. McCain, K. S.; Hanley, D. C.; Harris, J. M., Single-Molecule Fluorescence Trajectories for Investigating Molecular Transport in Thin Silica Sol-Gel Films. *Analytical Chemistry* **2003,** 75, (17), 4351-4359.

31. Takimoto, B.; Nabika, H.; Murakoshi, K., Single Molecular Observation of Hop Diffusion in a Lipid Bilayer at Metallic Nanogates. *The Journal of Physical Chemistry C* **2009,** 113, (8), 3127-3132.

32. Li, H.-W.; Park, H.-Y.; Porter, M. D.; Yeung, E. S., Single DNA Molecules as Probes of Chromatographic Surfaces. *Analytical Chemistry* **2005,** 77, (10), 3256-3260.

33. Park, H.-Y.; Li, H.-w.; Yeung, E. S.; Porter, M. D., Single Molecule Adsorption at Compositionally Patterned Self-Assembled Monolayers on Gold: Role of Domain Boundaries. *Langmuir* **2006,** 22, (9), 4244-4249.

34. Kang, S. H.; Shortreed, M. R.; Yeung, E. S., Real-Time Dynamics of Single-DNA Molecules Undergoing Adsorption and Desorption at Liquid−Solid Interfaces. *Analytical Chemistry* **2001,** 73, (6), 1091-1099.

35. He, Y.; Li, H.-W.; Yeung, E. S., Motion of Single DNA Molecules at a Liquid−Solid Interface As Revealed by Variable-Angle Evanescent-Field Microscopy. *The Journal of Physical Chemistry B* **2005,** 109, (18), 8820-8832.

36. Donner, S.; Li, H.-W.; Yeung, E. S.; Porter, M. D., Fabrication of Optically Transparent Carbon Electrodes by the Pyrolysis of Photoresist Films: Approach to Single-Molecule Spectroelectrochemistry. *Analytical Chemistry* **2006,** 78, (8), 2816-2822.

37. Rant, U.; Arinaga, K.; Fujita, S.; Yokoyama, N.; Abstreiter, G.; Tornow, M., Dynamic Electrical Switching of DNA Layers on a Metal Surface. *Nano Letters* **2004,** 4, (12), 2441-2445.

38. Kaiser, W.; Rant, U., Conformations of End-Tethered DNA Molecules on Gold Surfaces: Influences of Applied Electric Potential, Electrolyte Screening, and Temperature. *Journal of the American Chemical Society* **2010,** 132, (23), 7935-7945.

39. Hansen, W., Electric Fields Produced by the Propagation of Plane Coherent Electromagnetic Radiation in a Stratified Medium. *Journal of the Optical Society of America* **1968,** 58, (3), 380-390.

40. Mortara, L.; Fowler, A., Evaluations of CCD: Performance for astronomical use. *Proc. SPIE* **1981,** 290, 28-33.

41. Efron, B., Bootstrap Methods: Another Look at the Jackknife. *The Annals of Statistics* **1979,** 7, (1), 1-26.

42. Heider, E. C.; Peterson, E. M.; Barhoum, M.; Gericke, K. H.; Harris, J. M., Quantitative fluorescence microscopy to determine molecular occupancy of phospholipid vesicles. *Anal Chem* **2011,** 83, (13), 5128-36.

43. Dawson, J. R.; Harpst, J. A., Light scattering and hydrodynamic properties of linear and circular bacteriophage lambda DNA. *Biopolymers* **1971,** 10, (12), 2499-2508.

44. Liu, M. K.; Giddings, J. C., Separation and measurement of diffusion coefficients of linear and circular DNAs by flow field-flow fractionation. *Macromolecules* **1993,** 26, (14), 3576-3588.

45. Robertson, R. M.; Laib, S.; Smith, D. E., Diffusion of isolated DNA molecules: Dependence on length and topology. *Proceedings of the National Academy of Sciences* **2006,** 103, (19), 7310-7314.

46. Larsson, A.; Carlsson, C.; Jonsson, M.; Albinsson, B., Characterization of the Binding of the Fluorescent Dyes YO and YOYO to DNA by Polarized Light Spectroscopy. *Journal of the American Chemical Society* **1994,** 116, (19), 8459-8465.

47. Fulmer, A. W.; Benbasat, J. A.; Bloomfield, V. A., Ionic strength effects on macroion diffusion and excess light-scattering intensities of short DNA rods. *Biopolymers* **1981,** 20, (6), 1147-1159.

48. Gouy, L. G., Sur la constitution de la charge électrique à la surface d'un électrolyte *J. Phys. Theor. Appl.* **1910,** 9, (1), 457-467.

49. Chapman, D. L., A contribution to the theory of electrocapillarity. *Phil. Mag.* **1913,** 25, (148), 475-481.

50. Williams, G. D.; Soper, A. K.; Skipper, N. T.; Smalley, M. V., High-Resolution Structural Study of an Electrical Double Layer by Neutron Diffraction. *The Journal of Physical Chemistry B* **1998,** 102, (45), 8945-8949.

51. Tikhonov, A. M., Water Density in the Electric Double Layer at the Insulator/Electrolyte Solution Interface. *The Journal of Physical Chemistry B* **2006,** 110, (6), 2746-2750.

52. Sun, J.; Velamakanni, B. V.; Gerberich, W. W.; Francis, L. F., Aqueous latex/ceramic nanoparticle dispersions: colloidal stability and coating properties. *Journal of Colloid and Interface Science* **2004,** 280, (2), 387-399.

53. Tseng, W. J.; Tzeng, F., Effect of ammonium polyacrylate on dispersion and rheology of aqueous ITO nanoparticle colloids. *Colloids and Surfaces A: Physicochemical and Engineering Aspects* **2006,** 276, (1-3), 34-39.

54. Smith, S. B.; Bendich, A. J., Electrophoretic charge density and persistence length of DNA as measured by fluorescence microscopy. *Biopolymers* **1990,** 29, (8-9), 1167-1173.

55. Schellman, J. A.; Stigter, D., Electrical double layer, zeta potential, and electrophoretic charge of double-stranded DNA. *Biopolymers* **1977,** 16, (7), 1415-34.

56. Fogarty, K.; McPhee, J. T.; Scott, E.; Van Orden, A., Probing the Ionic Atmosphere of Single-Stranded DNA Using Continuous Flow Capillary Electrophoresis and Fluorescence Correlation Spectroscopy. *Analytical Chemistry* **2008,** 81, (1), 465-472.

57. Verwey, E. J. W., Theory of the Stability of Lyophobic Colloids. *The Journal of Physical and Colloid Chemistry* **1947,** 51, (3), 631-636.

58. Derjaguin, B. V.; Landau, L., Theory of the stability of strongly charged lyophobic sols and of the adhesion of strongly charged particles in solutions of electrolytes. *Acta Physiochim. U.R.S.S.* **1941,** 14, (633).

59. Bhattacharjee, S.; Elimelech, M., Surface Element Integration: A Novel Technique for Evaluation of DLVO Interaction between a Particle and a Flat Plate. *Journal of Colloid and Interface Science* **1997,** 193, (2), 273-285.

60. Heaton, R. J.; Peterson, A. W.; Georgiadis, R. M., Electrostatic surface plasmon resonance: Direct electric field-induced hybridization and denaturation in monolayer nucleic acid films and label-free discrimination of base mismatches. *Proceedings of the National Academy of Sciences* **2001,** 98, (7), 3701-3704.

61. Johnson, R. P.; Gao, R.; Brown, T.; Bartlett, P. N., The effect of base-pair sequence on electrochemically driven denaturation. *Bioelectrochemistry* **2012,** 85, (1), 7-13.

62. Quartin, R. S.; Wetmur, J. G., Effect of ionic strength on the hybridization of oligodeoxynucleotides with reduced charge due to methylphosphonate linkages to unmodified oligodeoxynucleotides containing the complementary sequence. *Biochemistry* **1989,** 28, (3), 1040-1047.

FIGURE CAPTIONS

Figure 1. Sample flow cell assembled into microscope stage holder with through-the-objective TIRF illumination.

Figure 2. a) Sample images of 10.5 pM DNA, 0.28 mM ionic strength solution over ITO, acquired ~120 s after indicated potential step versus Ag\AgCl ref. electrode. b) Molecules located by counting algorithm in 0.8 V sample image; scale bar is 10 μm.

Figure 3. Average DNA molecule counts in the 70 μm x 70 μm image area after potential step with Poisson-Boltzmann fit using equation 4 (solid line) for ionic strengths of (a) 8.5 μM (black squares), (b) 0.28 mM (red circles), (c) 3.2 mM (blue triangles), and (d) 30 mM (green diamonds) with bulk solution DNA concentrations of 5.3, 10.5, 21, and 42 pM, respectively. (e) The relative population excess in the double layer, $[N_{DET} - (N_E^0 - N_D^0)]/N_D^0$ (points) is compared to the Boltzmann factor, $\exp[-\beta(E - \varphi_{OHP}^0)]$ (lines).

Figure 4. DNA diffusion coefficients, D, plotted versus applied potential for 8.4 μM (black squares), 0.28 mM (red circles), and 3.2 mM (blue triangles) ionic strengths. The dashed line is the measured bulk solution DNA diffusion coefficient. Error bars are two standard deviations of the mean.

Figure 5. Boltzmann potential sensitivity parameter, $-\beta$, from the fit of data in Figure 3 to Equation 7, plotted versus Debye length , κ^{-1}.

Figure 6. Fraction of DNA population in the evanescent detection volume influenced by the double-layer region, N_D^0 / N_E^0 from fit of the data in Figure 3 to Equation 7, plotted versus Debye length, κ^{-1}.

Figure 7. DNA concentration factor, N_{DET}/N_E^0 , plotted versus applied potential for 8.4 μM (black squares), 0.28 mM (red circles), 3.2 mM (blue triangles), and 30 mM (green triangles) electrolyte ionic strengths. Solid lines are models of Gouy-Chapman double-layer ion concentration integrated through the evanescent detection region (150 nm from surface) fit to N_{DET}/N_E^0 with net DNA charge in electron equivalents of Z = −0.79, −0.79, −0.70, and −0.61, respectively.

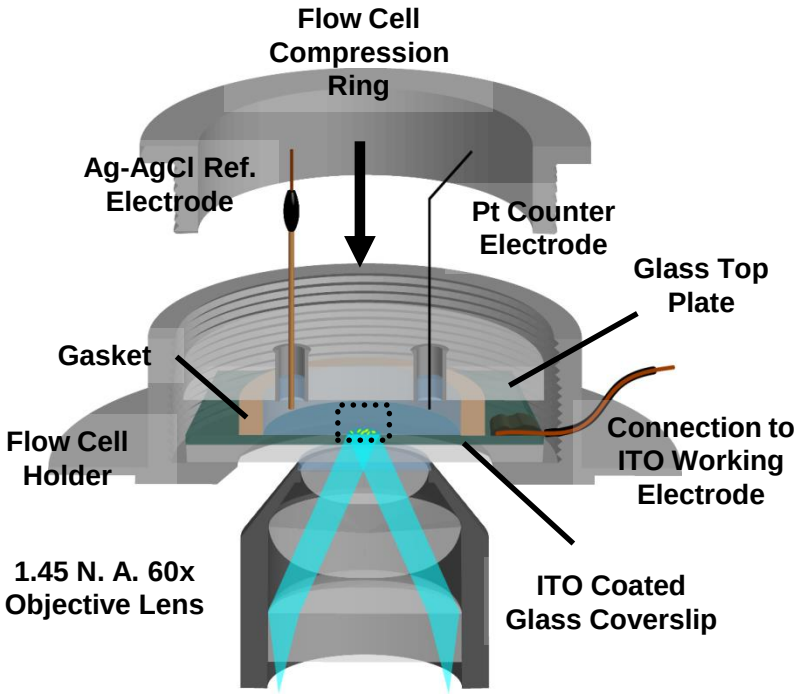
Flow Cell
Compression
Ring
Ag-AgCl Ref.
Electrode
Pt Counter
Electrode
Glass Top
Plate
Gasket
Flow Cell
Holder
Connection to
ITO Working
Electrode
1.45 N. A. 60x
Objective Lens
ITO Coated
Glass Coverslip

Figure 1

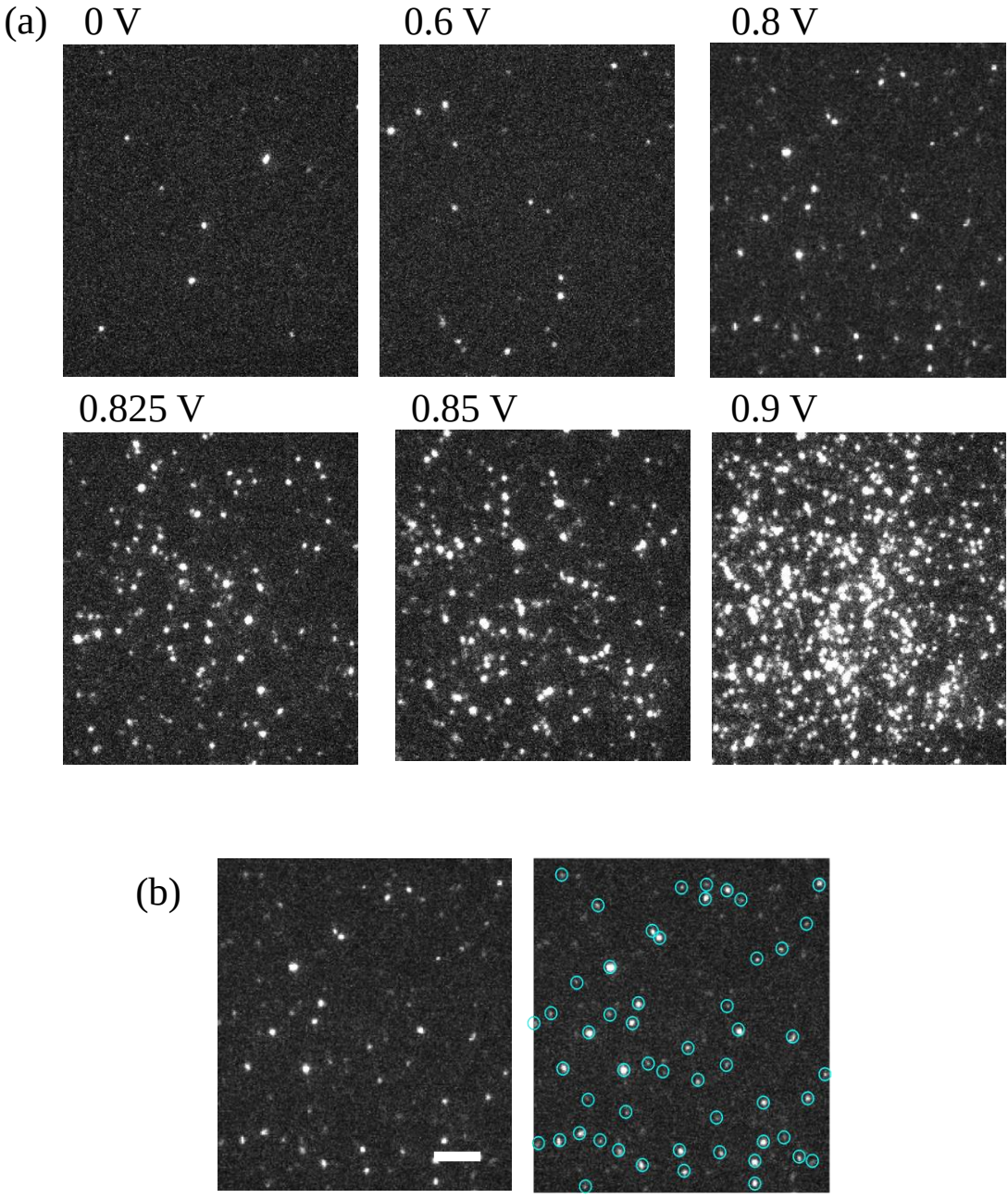

Figure 2

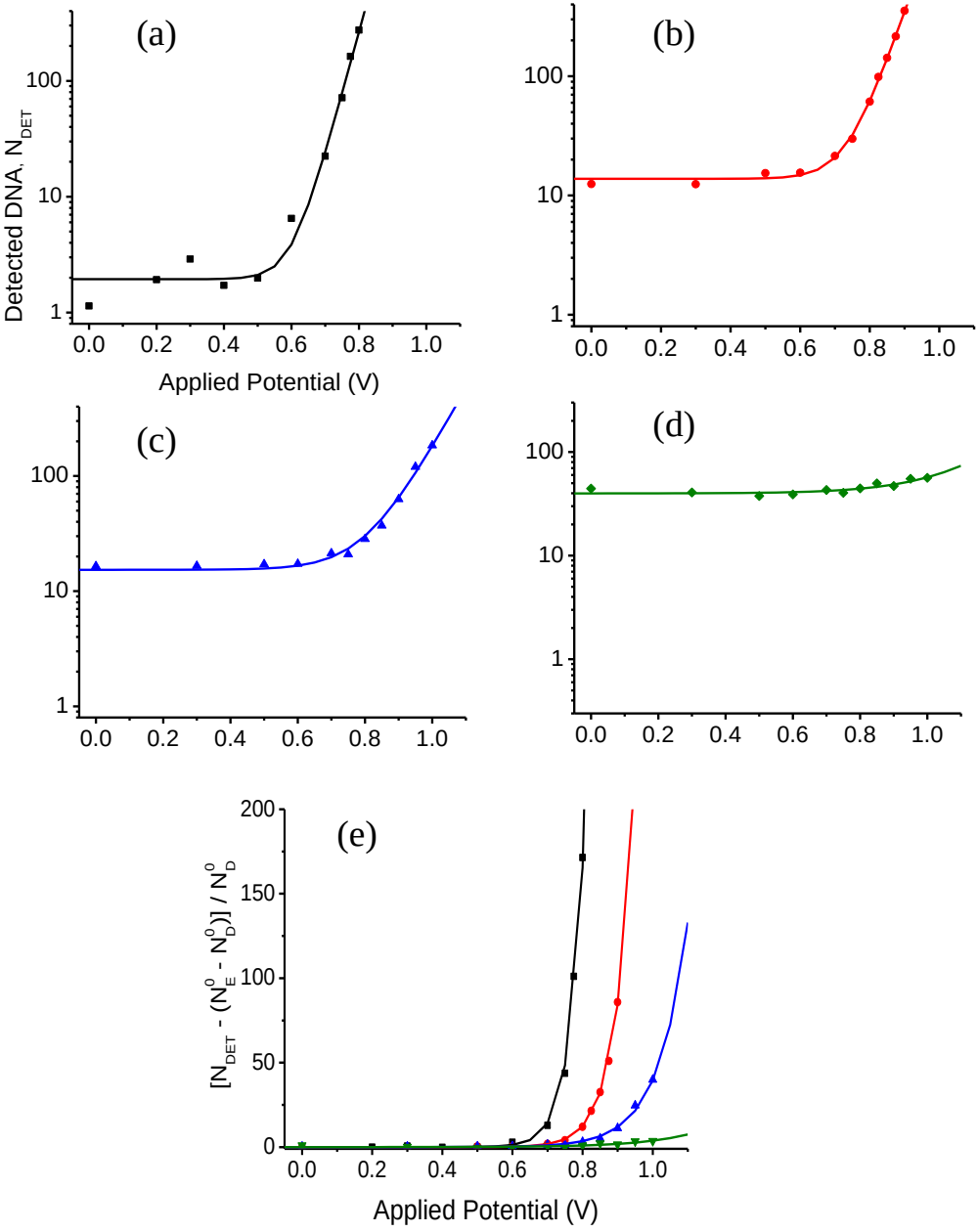
(a)
(b)
(c)
(d)
(e)
Detected DNA, N_{DET}
Applied Potential (V)
$[N_{DET} - (N_E^0 - N_D^0)] / N_D^0$
100
10
1
200
150
50
0
0.0
0.2
0.4
0.6
0.8
1.0

Figure 3

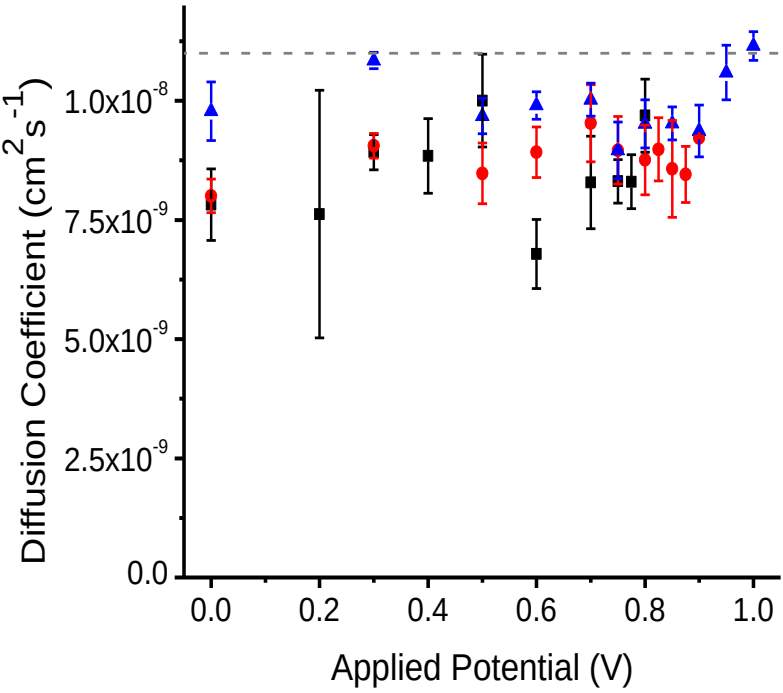
Diffusion Coefficient (cm^2 s^{-1})
1.0x10^{-8}
7.5x10^{-9}
5.0x10^{-9}
2.5x10^{-9}
0.0
0.0
0.2
0.4
0.6
0.8
1.0
Applied Potential (V)

Figure 4

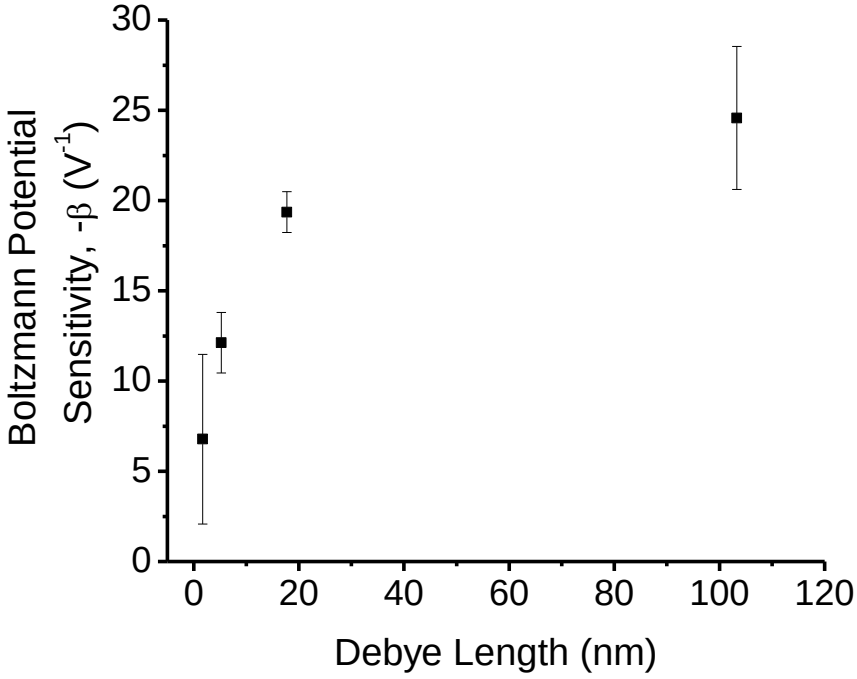
Boltzmann Potential
Sensitivity, -β (V-1)
30
25
20
15
10
5
0
0
20
40
60
80
100
120
Debye Length (nm)

Figure 5

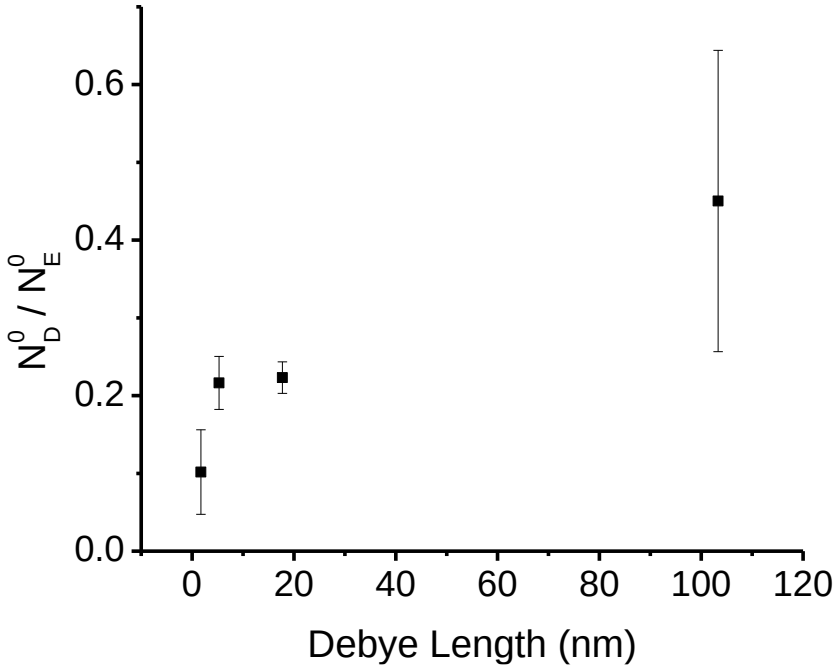

Figure 6

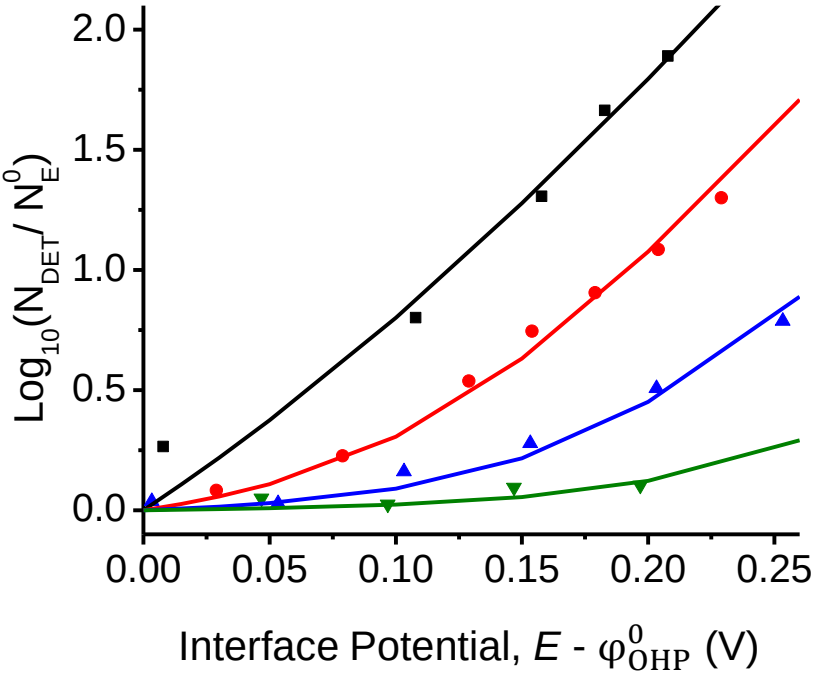
2.0
1.5
1.0
0.5
0.0
0.00
0.05
0.10
0.15
0.20
0.25
Log10(NDET / NE0)
Interface Potential, E - φOHP0 (V)

Figure 7

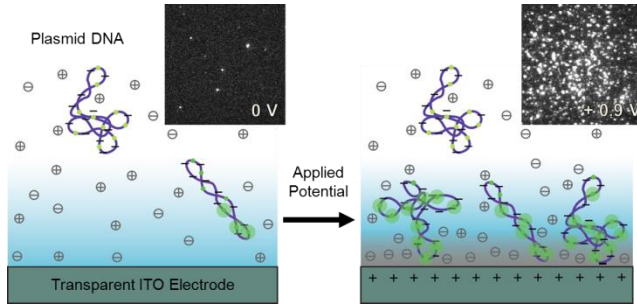

Table of Contents Graphic